Organic Photovoltaic Cell-Powered Backscatter Communication System: A Compact Design

Adrian Salustri*, Alexander Williams*, Mathew Salas*, Hassan Khaniani[†], Mostafa Hassanalian[‡], Pedram Roghanchi[§], Sihua Shao*

*Department of Electrical Engineering, New Mexico Tech, Socorro, NM 87801. Email: sihua.shao@nmt.edu †PRRC, New Mexico Tech, Socorro, NM 87801. Email: hassan.khaniani@nmt.edu

Abstract—The paper outlines the design, prototyping, and simulation processes involved in creating a compact radio frequency (RF) backscatter communication system, powered by Organic Photovoltaic (OPV) cells. This system is integral to a mine rescue operation, particularly useful in scenarios where miners are trapped due to accidents. In such situations, a rescue drone, equipped with a searchlight and the discussed communication system, takes the lead in the assisted escape mission for miners. The drone establishes duplex communication with the miners through a battery-free, wearable transponder device. Initial experiments employing a RF backscatter testbed - which utilizes both software-defined radios and OPV cells - were conducted. These preliminary tests were crucial for assessing the conditions necessary for successful backscatter communication, as well as for evaluating the energy-harvesting performance of the system. Findings from these experiments indicate that the device can operate battery-free, powered solely by OPV cells, even under low illuminance levels of less than 75 lux. In the pursuit of crafting the device in a compact form, a co-design initiative was launched. This effort focused on developing a meander dipole antenna in tandem with the OPV cells, targeting a resonant frequency of 912 MHz. Simulation results, obtained from ANSYS HFSS, revealed significant changes in antenna impedance and S parameters yet minimal impact on the radiation pattern of the antenna with the integration of the layered OPV structure.

Index Terms—Backscatter communications, energy harvesting, wireless power transfer, wearable device, wireless communications testbed, measurements.

I. Introduction

Underground mining inherently possesses significant dangers. Accidents while working can trap miners underground, requiring risky rescue endeavors. Historically, the risks to rescuers have been real; since the late 1800s, the United States has witnessed the loss of over 200 mine rescuers during missions to aid their trapped colleagues. In light of this, recent initiatives have sought to amplify the level of automation within search and rescue operations, aiming to enhance safety and efficacy during these critical missions.

This work forms a segment of a project funded by the National Institute for Occupational Safety and Health (NIOSH), aimed at devising a robotic system to locate and assist miners

Corresponding author: Sihua Shao, sihua.shao@nmt.edu.

The work is supported by National Science Foundation (NSF) CNS-2245747 and National Institute for Occupational Safety & Health (NIOSH) U60 OH012351-01.

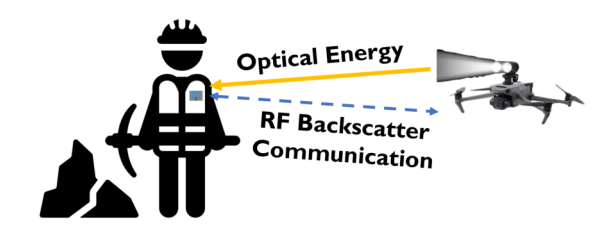


Fig. 1: Trapped miner uses the OPV powered RF backscatter tag to communicate with RF reader carried by a intelligent rescue drone.

entrapped subsequent to an accident, all while human first responders are en route. A pivotal feature of the robotic system is its capacity to establish swift and dependable wireless communication with the confined miners. This wireless connection enables the advanced rescue system to obtain valuable feedback from miners involved in self-escape activities, such as conveying their level of distress. To realize this, we propose outfitting miners with a wearable transponder device, thereby facilitating communication with rescue drones during mine emergency situations.

Designing a wearable, safety-critical electronic system for utilization in an underground mine presents substantial challenges. Firstly, the harsh physical environment underground necessitates a device that is not only compact but also rugged, ensuring it can be securely worn by a miner during work. The conditions only deteriorate during an emergency, with factors such as dust or smoke from an explosion or cavein further compromising signal integrity and visibility [1]. Additionally, human operators, who might typically mitigate communication challenges, could be disoriented or incapacitated. Even with the support of robotics, locating trapped miners can require many exhaustive hours. There's a potential risk of power depletion in a battery-powered device exacerbate these scenarios. Consequently, our design endeavors focus on achieving a "battery-free" design, enabling the device to fully operate through ambient energy harvesting when necessary.

Backscatter communication emerges as a prevalent strategy for establishing a link in scenarios where one side experiences strict size, weight, and power (SWaP) constraints. Instead of embedding a power-intensive transmitter in both devices, an

[‡]Department of Mechanical Engineering, New Mexico Tech, Socorro, NM 87801. Email: mostafa.hassanalian@nmt.edu

[§]Department of Mining Engineering, University of Kentucky, Lexington, KY 40508. Email: pedram.roghanchi@uky.edu

asymmetric channel is devised: one device (the interrogator) employs a potent transmitter, while the other (the tag) merely reflects the energy back, modulating it to encode information. This scheme underpins the operation of RFID tags [2], and is similarly exploited for optical [3] and ultrasonic waves [4].

In this study, our focus is dedicated to addressing power requirements by incorporating a flexible, organic photovoltaic (OPV) cell to enhance an RF energy harvesting approach (Fig. 1). This integration is sensible, given that RF and optical waves — due to their distinct wavelengths — propagate differently within the mine. In emergency scenarios, it's conceivable that RF energy may be attenuated to a degree insufficient to power the device. However, the optical power emitted from the rescue drone's searchlight *is* enough. Therefore, by including a PV cell, we establish a redundancy in the power supply, thereby improving the system's robustness.

The integration of a PV cell presents unique challenges. Mines typically exhibit low light levels, necessitating a device that's optimized for minimal illuminance. Moreover, the use of glass or silicon crystals is not desirable in mine environments due to the risk of breakage. Additionally, the size prerequisite demands that the backscatter antenna be intricately integrated with the PV cell, thereby complicating antenna design. These collective requirements guide our choice to employ an OPV cell. This emerging technology proves to be more adaptable to low-power, low-illumination energy harvesting across arbitrary geometries [5].

In Sec.II, we explore pertinent literature concerning the enhancement of energy harvesting functions in RFID. Our discussion regarding RF backscatter modulation and the energy harvesting mechanism is in Sec.III. The conceptualization of the compact design, integrating OPV and antenna, is outlined in Sec.IV. Sec.V showcases a proof-of-concept testbed, employed to evaluate conditions required for active backscatter communication. Meanwhile, the compact design undergoes simulation in Ansys HFSS, with results and discussions presented in Sec. VI.

The contributions of our work are summarized below:

- We design an energy-harvesting solution that enhances RF backscatter, utilizing OPV augmentation.
- The prototype communicates based on frequency shift keying under minimal illuminance as low as 75 lux.
- A compact integration of OPV cells and a meandered antenna is designed.
- We conduct Ansys HFSS simulations to evaluate the antenna impedance, S parameter, and radiation pattern.

II. RELATED WORK

There is a long history of work augmenting and improving energy harvesting systems in the context of RFID. The performance of passive RFID systems are typically limited by the efficiency of the power harvesting circuitry. This is because modern radio transceivers can successfully decode signals on the order of -70dBm [6], but the low-power circuitry on the tag needs around -10dBm (100 μ W) to function.

RF energy harvesting techniques and applications have been explored for two decades [7], [8]. However, there are also many other possible energy harvesting schemes beyond RF as explored in [9]. In particular, [10]–[13] studied RF backscatter systems using traditional PV cells.

Compared to traditional PV cells, the flexibility, weight, and marginal cost of OPV cells make them a very promising technology for battery-free IoT devices going forward [14]. OPVs are also more efficient than a comparable amorphous silicon cell in low light, making them especially useful for the low illuminance of underground mines [15]. Recent development of ink-jet printed OPVs let electrical designers construct arbitrary geometries of OPV cells for use in their designs [16]. This allows for unprecedented integration of PV energy harvesting into RF antenna assemblies. To the best of our knowledge, no existing literature has explored OPV-powered backscatter under very low illumination levels (<100 lux).

III. SYSTEM OVERVIEW

A. RF Backscatter Modulation

In this study, our concentration is solely anchored on the backscatter uplink design. The interrogator releases a continuous RF signal, serving as the carrier wave for the backscatter communication. The tag, either a passive or semi-passive device, reflects the RF signals originating from the interrogator. Its fundamental role is to modulate this reflected signal, encoding information in the process. Additionally, in a device outfitted with RF energy harvesting, the tag also absorbs energy from the incident carrier wave generated by the interrogator.

The backscatter modulator functions by dynamically changing the load impedance connected to the tag's antenna. Recall the reflection coefficient for a terminated lossless transmission line Γ is a function of this load impedance as below

$$\Gamma = \frac{Z_0 - Z_L}{Z_0 + Z_L}$$

where Z_0 is the antenna impedance and Z_L is the load impedance seen by the antenna [17]. Note that

$$\Gamma = \begin{cases} 1 & \text{if } Z_L = 0 \\ -1 & \text{if } Z_L = \infty \\ 0 & \text{if } Z_L = Z_0 \\ j\frac{X_L}{R_L} & \text{if } Z_L = Z_0^* \end{cases} \quad \text{(Max Power Transfer)}$$

By rapidly toggling Z_L between discrete loads using a microcontroller and RF switch, we effectively multiply the reflected wave by a square wave in the time domain, correlating to a shift in the frequency domain. Adjusting the switching frequency of the square wave enables us to implement frequency shift keying (FSK) modulation. Moreover, FSK modulation also offers a direct solution to mitigate self-interference by filtering out the continuous carrier signal.

Note that in the implementation of an active or non-RF powered FSK backscattering, it is optimal to toggle between open and closed Z_L , as there is no necessity to absorb power

from the interrogating RF signal. If the device employs RF energy harvesting, Z_L must switch between open and Z_0^* to ensure maximum power transfer. More complex modulation schemes can optimize the duration where the switch is in the state of maximum power absorption [18].

B. Energy Harvesting

The energy-harvesting power supply circuit is depicted in Fig. 2, illustrating both RF and OPV energy harvesting subsystems. The prototype (Sec.V) excludes RF energy harvesting in order to assess the capability of OPV-only energy harvesting. However, during the antenna design (Sec.IV) and simulations (Sec. VI), the RF energy harvesting module is taken into consideration. An RF energy harvester typically encompasses a rectifying circuit and a charge pump boost circuit, followed by a rectifying diode, which converts the alternating current (AC) derived from the absorbed RF signals into direct current (DC) [19]. To facilitate maximum power transfer, the input impedance of the rectifying circuit must be conjugate matched to the antenna. Often, it is practical to match the antenna impedance to the circuit via antenna meandering, rather than employing a traditional RLC matching circuit [20].

For the OPV, three main submodules are utilized. Initially, there is the PV cell, which can either be composed of amorphous silicon or organic polymer. Subsequently, this cell is cascaded with a low forward bias Schottky diode to protect against reverse current discharge. Additionally, a substantial capacitor (68 μ F) is incorporated to store and stabilize the energy derived from the harvester. A low drop-out linear voltage regulator [21] yields a 2V supply designated for the microcontroller. Through the employment of the Enable pin feature and a feedback network, controlled hysteresis is introduced to the voltage regulator. This configuration establishes a defined band within which the output voltage may vary without prompting the regulator to rapidly toggle states.

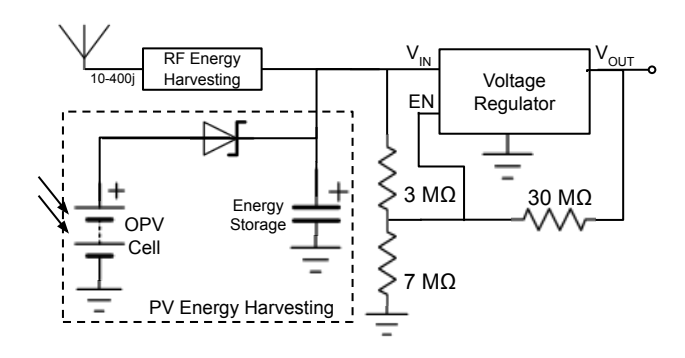


Fig. 2: Schematic diagram of the energy harvesting system

IV. INTEGRATED OPV AND MEANDERED DIPOLE

In pursuit of a compact design that integrates an antenna and OPV cells, we investigate the viability of layering the OPV cells atop the antenna and RF circuitry. While the design of meandered dipole antennas is well-established, it is important to understand the impact of the OPV cell on

the antenna. Given that the radiation pattern and antenna impedance are highly susceptible to alterations in their near-field surroundings, iterative simulations become crucial to make adjustments for any packaging or interfering materials. Although any material in proximity to the antenna will alter its performance, the structure of the OPV proves particularly disruptive due to the organic conductors connecting the OPV material and the extended traces transmitting harvested energy to the device.

We opt for the meandered dipole geometry due to its spatial efficiency and the capability to tune the antenna impedance to the RF frontend by modifying the geometry. The overall 3D structure of the integrated design is illustrated in Fig.3a. To evaluate the impact of varying OPV dimensions on the antenna performance, we conduct ANSYS HFSS simulations based on distinct values of the parameters depicted in Fig.3b. Table I summarizes the parameter values utilized in the simulation, with the enlightening results being discussed in Sec. VI.

TABLE I: Antenna Simulation Parameters

Parameter	UHF Antenna	Tuned Antenna
Target Frequency	912MHz	912MHz
H	47mm	47mm
W	12mm	47mm
h	10mm	3.6mm
w	9mm	6.1mm
$h_{ m trim}$	1mm	6mm
$h_{ m feed}$	10mm	10mm
t	$500\mu\mathrm{m}$	$500\mu\mathrm{m}$
d	4.5mm	4.5mm
$d_{ m dc}$	17.7 mm	22mm
OPV ϵ_r	4	4
PET ϵ_r	3.59861	3.59861
Conductive Polymer σ/m	3000 S/m	3000 S/m
Z_0	10-350j	10-350j

V. EXPERIMENTS

A proof-of-concept testbed was implemented to examine the RF backscatter functionality and characterize the energyharvesting performance. Fig. 4c presents the schematic diagram of the testbed, which encompasses a backscatter tag and an interrogator, seperated at variable distances.

The tag (Fig. 4a) was implemented using a COTS 900 MHz monopole antenna connected to a Skyworks single pole double throw (SPDT) RF switch [22] evaluation board. Each terminal of the switch was terminated with an open circuit ($Z_L = \infty$) or a shorting cap ($Z_L = 0$). The switch was controlled by an ATTiny20 8-bit microcontroller running on the lowest power mode that enables hardware timers. The tag used a 3V, 160μ W OPV panel from Dracula Technologies [23] attached to the front for power harvesting. The dimensions of the OPV cells were W = 7.5mm by H = 57mm, with a total of 6 cells.

The interrogator (Fig. 4b) comprised a custom lighting system, two circularly polarized antennas [24], and an USRP N210 software-defined radio (SDR) [25]. The lighting system employed a set of LEDs powered by a 12V DC source. The lighting system was mounted between the two antennas configured as a transmitter (Tx) and receiver (Rx) for the

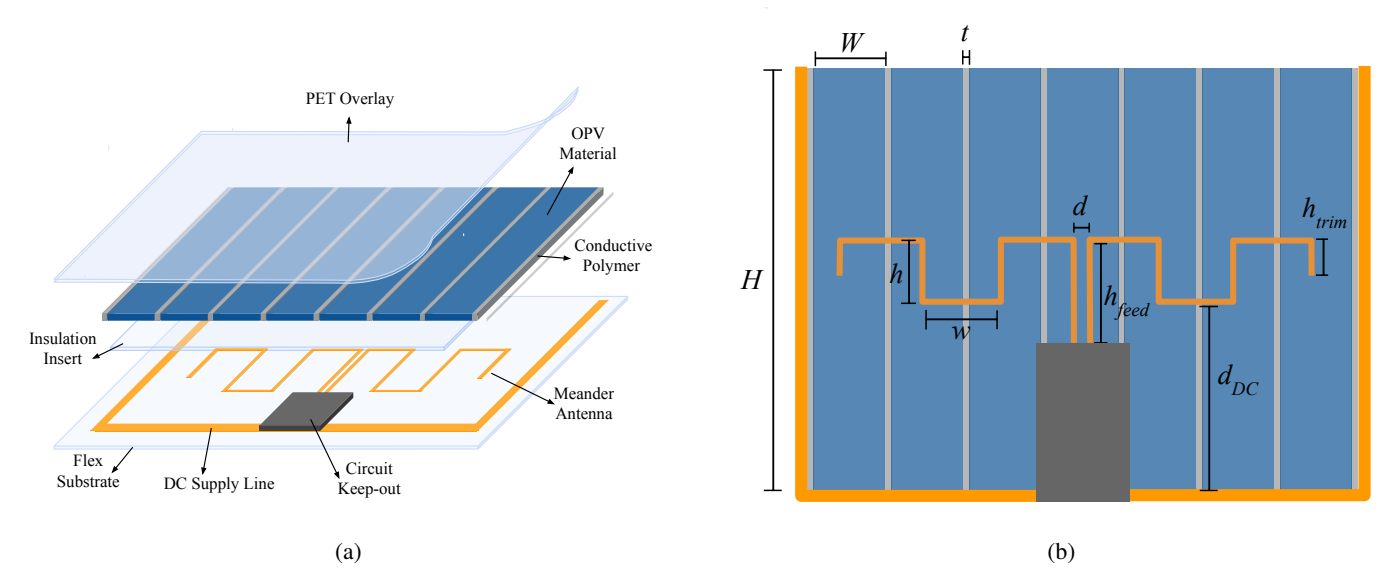


Fig. 3: (a) 3D layered structure of the compact design and (b) the dimensions of the OPV cells and meandered antenna.

SDR. The SDR and light were controlled from the same GNU Radio flowgraph, allowing synchronization between the LEDs and antenna for the purpose of precise cold start time measurement.

A. RF Backscatter Communication

At the beginning of the trial, the transmitting antenna began emitting a carrier frequency at 900MHz. The backscatter tag had a 3 switch UI to select the modulation frequency. Utilizing FSK, the tag could transmit at frequencies of 98.3kHz, 122.7kHz, and 163.6kHz. The reflected signal was received by the Rx antenna, and the raw data was subsequently forwarded to the GNU Radio flowchart. This flowchart filtered each of the transmitted frequencies to ascertain which was being received. A threshold process was then applied to generate clean signal data, indicating both the detected frequency and the occurrence of the rising edge for that detection.

B. OPV Energy Harvesting

The performance of the power supply was characterized by the following metrics:

- Cold start time t_{cs} : The time required for the device to turn on after light is applied, starting with the stabilizing capacitor completely discharged.
- On-time t_{on}: Under low illuminance scenarios, it is likely
 the device will use more energy than can be continuously
 collected, and will therefore show power cycling behavior
 (intermittent transmission). In this case, t_{on} is the time
 the device is active before it must turn off to recharge.
- Off-time t_{off} : Similarly, t_{off} is the amount of time the device must be inactive until it has collected enough energy to turn on again. t_{off} is strictly less than t_{cs} because the stabilizing capacitor does not completely discharge during normal operation.
- Duty Cycle is defined as $\frac{t_{on}}{t_{on}+t_{off}} \times 100\%$.

An experiment was conducted to characterize the behavior of the prototype tag according to these metrics under various lighting conditions. To do this, the backscatter tag was programmed to transmit a constant frequency (98.3kHz) immediately on startup. At t=0 of each trial, the LED light and RF interrogator were enabled simultaneously.

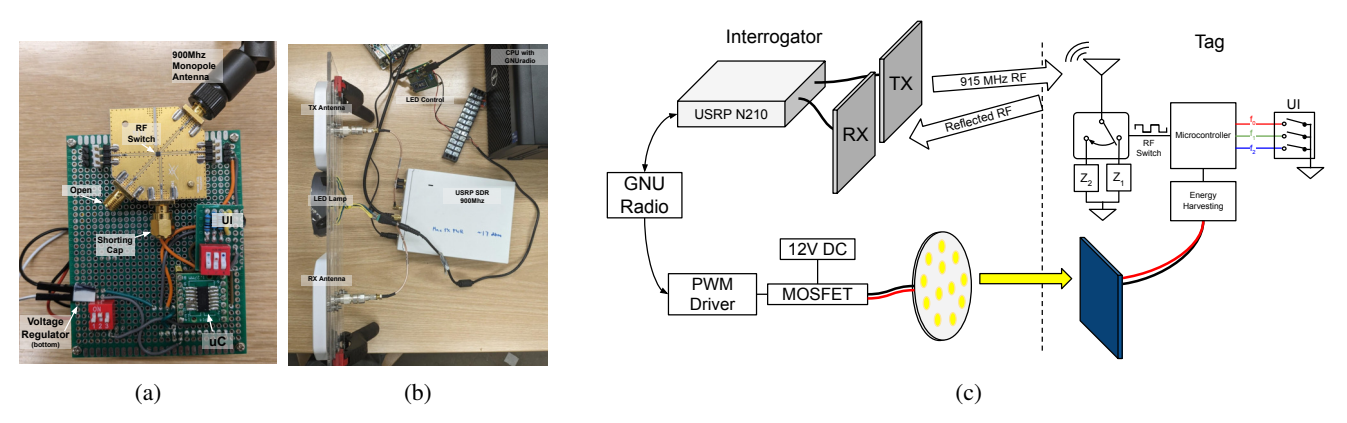


Fig. 4: (a) Prototype of backscatter tag, (b) prototype of RF reader with light, and (c) schematic diagram of the testbed.

The backscattered RF signal was recorded over 8 different illuminance levels. For each trial, the tag was positioned facing the lighting unit at a fixed distance, with an Extech LT300 lux meter mounted next the OPV cell to measure the incident light intensity. The illuminance was varied by changing the distance between the tag and interrogator. After each trial, the capacitor was shorted to ensure an uncharged state for accurate cold start measurements.

Fig. 6a is a representative output from a single trial. The signal processing used to construct this plot is shown in Fig. 5. After isolating the backscattered signal, a dynamic threshold (green trace) was calculated via a 1ms moving average, which then was compared to the RF signal magnitude (orange trace) to determine if the backscatter tag was transmitting. The resulting binary signal (blue trace) was analyzed to find t_{cs} , t_{on} , and t_{off} as marked.

Fig. 6c shows the results as a function of illuminance (in lux). We see that the cold start time decreases exponentially as a function of illuminance, as expected. At 75 lux, t_{cs} is 11.1 seconds, t_{on} is .172 seconds, t_{off} is 4.177 seconds and duty cycle is 4%.

Fig. 6b shows the role of hysteresis in power cycling behavior. This plot was constructed by measuring the OPV output voltage V_{OPV} and the regulator output voltage v_{reg} over 10 cycles at an illuminance of 200 lux. As shown by the time arrow, for $t < t_{cs}$ the capacitor charges until $V_{OPV} = V_{HI}$. Then the device turns on and starts drawing current which discharges the capacitor. After t_{on} seconds, $V_{OPV} = V_{LO}$ and the regulator shuts down. V_{OPV} starts to rise again, cycling like this indefinitely.

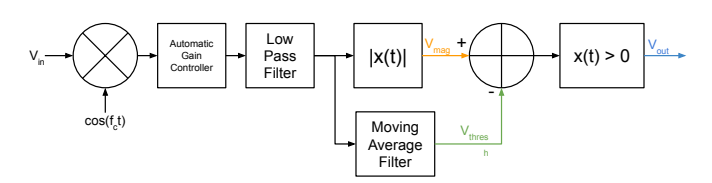


Fig. 5: The signal processing used to generate Fig. 6a (implemented in GNURadio)

VI. SIMULATIONS

Simulation results for the compact integrated design are depicted in Fig. 7. A 912MHz meandered dipole is simulated both with and without the presence of an OPV cell to illustrate the degradation. Three cases were evaluated: the meandered antenna suspended in free space (no OPV), the meandered antenna with the OPV cell, and a tuned meander antenna to re-achieve a 912MHz resonance. The analysis provides insight into the effects of introducing the OPV cell on the radiation pattern and behavior of the antenna. This behavior is of interest because it provides insights on the necessary changes needed to re-achieve a frequency within the permitted band.

The radiation pattern for each scenario is presented, along with the Z and S_{11} curves. In the return loss calculation, the presence of RF energy harvesting circuitry is accounted

for with an input impedance of 10-350j, a typical value for such circuits [26]. The introduction of the OPV leads to a decrease in the resonant frequency by more than 400 MHz. This is anticipated, as the introduction of conducting and semiconducting layers adjacent to the antenna introduces a considerable capacitive load. In order to use the antenna, the desired resonant frequency must be restored and the antenna impedance must be conjugate matched to the tag electronics. The results of tuning show that this can be addressed by modifying the h and w values of the meander antenna. It's noteworthy that the when testing the antenna with the OPV cell the changes in the azimuthal plane beam pattern shape are marginal, however the beam pattern in three dimensions exhibits more extreme deviations.

VII. CONCLUSION

In this work, we introduced and prototyped a battery-free RF backscatter device, powered by OPV cells. Successfully, the device communicates via an FSK modulated backscatter communication channel, even under low illuminance levels of 75lux. Through the employment of Ansys HFSS simulations, we observed that the compact, integrated design of OPV cells and a meandered antenna notably alters antenna impedance and resonant frequency, while largely preserving the radiation pattern. Further finding that it was possible to re-achieve the intended resonant frequency through simple modifications of the antenna's dimensions. Moving forward, our endeavors will focus on implementing RF energy harvesting and developing a power supply capable of dynamically switching between RF and OPV energy harvesting. The printability of modern OPV cells allows tighter integration's between RF and Optical Energy harvesting, and calls for further exploration of novel form factors to further miniaturize devices that cannot operate merely on RF energy.

REFERENCES

- M. Wagner and N. A. University, "Sunshine mine disaster." [Online]. Available: https://www.intermountainhistories.org/items/show/539
- [2] R. Want, "An introduction to RFID technology," *IEEE Pervasive Computing*, vol. 5, no. 1, pp. 25–33, 2006.
- [3] S. Shao, A. Salustri, A. Khreishah, C. Xu, and S. Ma, "R-VLCP: Channel modeling and simulation in retroreflective visible light communication and positioning systems," *IEEE Internet of Things Journal*, 2023.
- [4] Q. Wang, Q. Guan, J. Cheng, and Y. Tang, "Ultrasonic backscatter communication for implantable medical devices," 2022. [Online]. Available: https://arxiv.org/abs/2202.06440
- [5] P. P. Kumavat, P. Sonar, and D. S. Dalal, "An overview on basics of organic and dye sensitized solar cells, their mechanism and recent improvements," *Renewable and Sustainable Energy Reviews*, vol. 78, pp. 1262–1287, 2017.
- [6] D. M. Dobkin, "Chapter 3 Radio Basics For UHF RFID," in *The RF in RFID*, D. M. Dobkin, Ed. Burlington: Newnes, Jan. 2008, pp. 51–101. [Online]. Available: https://www.sciencedirect.com/science/article/pii/B9780750682091500036
- [7] M. Philipose, J. Smith, B. Jiang, A. Mamishev, S. Roy, and K. Sundara-Rajan, "Battery-free Wireless Identification and Sensing," *IEEE Pervasive Computing*, vol. 4, no. 1, pp. 37–45, 2005.
- [8] S. Mandal, "Far field RF power extraction circuits and systems," Ph.D. dissertation, Massachusetts Institute of Technology, 2004.

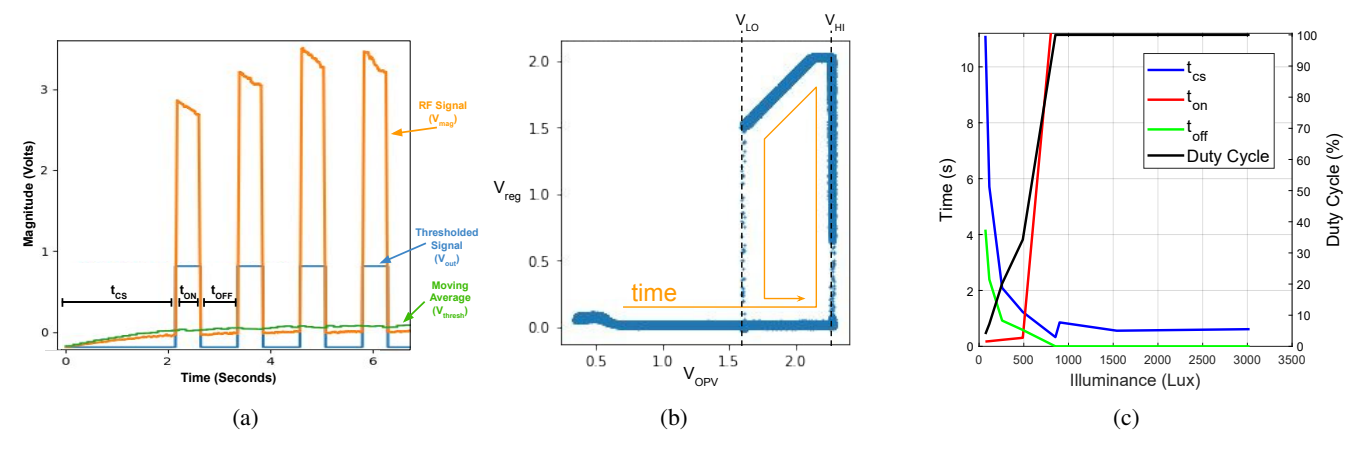


Fig. 6: (a) Typical time series of the backscattered signal, (b) The OPV voltage vs regulator output showing hysteresis in power supply, and (c) The performance of the power supply as a function of illuminance.

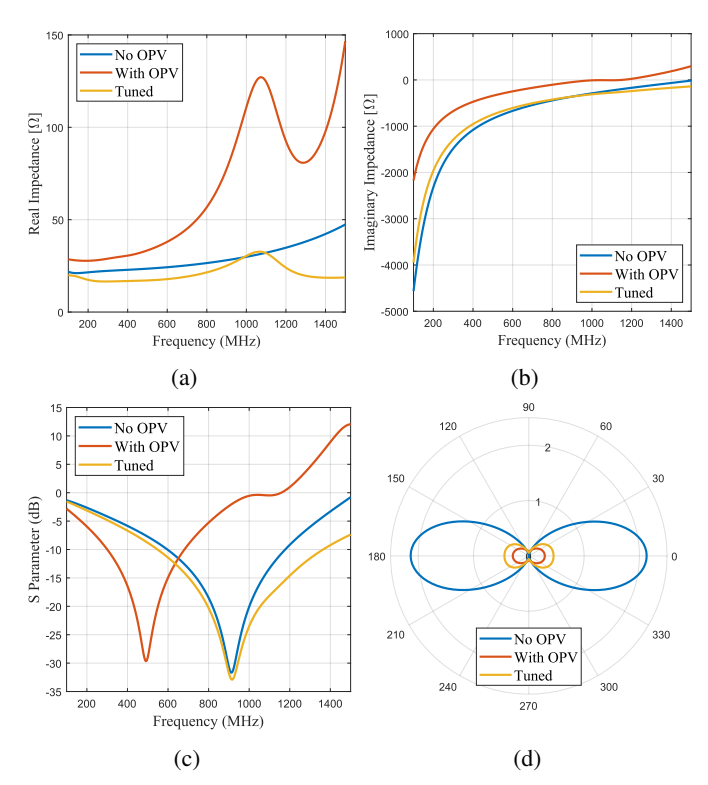


Fig. 7: (a) Real Impedance, (b) Imaginary Impedance, (c) Return loss (S_{11}) , and (d) Gain for $\phi=90^{\circ}$.

- [9] P. Choudhary, L. Bhargava, V. Singh, M. Choudhary, and A. k. Suhag, "A survey – Energy harvesting sources and techniques for internet of things devices," *Materials Today: Proceedings*, vol. 30, pp. 52–56, Jan. 2020. [Online]. Available: https://www.sciencedirect.com/science/ article/pii/S2214785320327309
- [10] A. E. Abdulhadi and R. Abhari, "Multiport UHF RFID-Tag Antenna for Enhanced Energy Harvesting of Self-Powered Wireless Sensors," *IEEE Transactions on Industrial Informatics*, vol. 12, no. 2, pp. 801–808, 2016
- [11] B. Molina-Farrugia, A. Rivadeneyra, J. Fernández-Salmerón, F. Martínez-Martí, J. Banqueri, and M. A. Carvajal, "Read Range Enhancement of a Sensing RFID Tag by Photovoltaic Panel," *Journal* of Sensors, 2017.
- [12] A. Ascher, M. Lehner, M. Eberhardt, and E. Biebl, "Improving the range

- of UHF RFID transponders using solar energy harvesting under low light conditions," *Advances in Radio Science*, vol. 13, pp. 81–86, 2015.
- [13] V. Iyer, H. Gaensbauer, T. L. Daniel, and S. Gollakota, "Wind dispersal of battery-free wireless devices," *Nature*, vol. 603, no. 7901, pp. 427– 433, 2022.
- [14] Y. Aoki, "Photovoltaic performance of Organic Photovoltaics for indoor energy harvester," *Organic Electronics*, vol. 48, pp. 194–197, Sep. 2017. [Online]. Available: https://www.sciencedirect.com/science/ article/pii/S1566119917302203
- [15] E. K. Solak and E. Irmak, "Advances in organic photovoltaic cells: a comprehensive review of materials, technologies, and performance," *RSC Advances*, vol. 13, no. 18, pp. 12 244–12 269. [Online]. Available: https://www.ncbi.nlm.nih.gov/pmc/articles/PMC10114284/
- [16] K. Y. Mitra, A. Alalawe, S. Voigt, C. Boeffel, and R. R. Baumann, "Manufacturing of All Inkjet-Printed Organic Photovoltaic Cell Arrays and Evaluating Their Suitability for Flexible Electronics," *Micromachines*, vol. 9, no. 12, p. 642, Dec. 2018. [Online]. Available: https://www.ncbi.nlm.nih.gov/pmc/articles/PMC6316076/
- [17] K. Kurokawa, "Power Waves and the Scattering Matrix," *IEEE Transactions on Microwave Theory and Techniques*, vol. 13, no. 2, pp. 194–202, Mar. 1965. [Online]. Available: https://ieeexplore.ieee.org/document/1125964
- [18] D. M. Dobkin, "Chapter 8 UHF RFID Protocols," in *The RF in RFID*, D. M. Dobkin, Ed. Burlington: Newnes, Jan. 2008, pp. 361–444. [Online]. Available: https://www.sciencedirect.com/science/article/pii/B9780750682091500085
- [19] Z. Xu, A. Khalifa, A. Mittal, M. Nasrollahpourmotlaghzanjani, R. Etienne-Cummings, N. X. Sun, S. S. Cash, and A. Shrivastava, "Analysis and Design Methodology of RF Energy Harvesting Rectifier Circuit for Ultra-Low Power Applications," *IEEE Open Journal of Circuits and Systems*, vol. 3, pp. 82–96, 2022.
- [20] K. Rao, P. Nikitin, and S. Lam, "Antenna design for UHF RFID tags: a review and a practical application," *IEEE Transactions on Antennas and Propagation*, vol. 53, no. 12, pp. 3870–3876, 2005.
- [21] "TCR3UF20A,LM(CT Toshiba | Mouser." [Online]. Available: https://www.mouser.com/ProductDetail/757-TCR3UF20ALMCT
- [22] "Skyworks | Products Details." [Online]. Available: https://www.skyworksinc.com/Products/Switches/SKY13314-374LF
- [23] "Applications | Dracula Technologies," Jul. 2022. [Online]. Available: https://dracula-technologies.com/applications/
- [24] "Laird S9025PL/S8655PL (LHCP) Outdoor RFID Antenna (FCC/ETSI)." [Online]. Available: https://www.atlasrfidstore.com/laird-s9025pl-s8655pl-lhcp-outdoor-rfid-antenna-fcc-etsi/
- [25] E. R. Brand, a National Instruments, "USRP N210 Software Defined Radio (SDR)." [Online]. Available: https://www.ettus.com/all-products/ un210-kit/
- [26] G. Marrocco, "The art of UHF RFID antenna design: impedance-matching and size-reduction techniques," *IEEE Antennas and Propagation Magazine*, vol. 50, no. 1, pp. 66–79, 2008.